Cytotoxicity of 1-deoxysphingolipid unraveled by genome-wide genetic screens and lipidomics in *Saccharomyces cerevisiae*

A. Galih Haribowo[a], J. Thomas Hannich[a], Agnès H. Michel[b], Márton Megyeri[c,d], Maya Schuldiner[c], Benoît Kornmann[b], and Howard Riezman[a,*]

[a]NCCR Chemical Biology and Department of Biochemistry, University of Geneva, 1211 Geneva, Switzerland; [b]Department of Biochemistry, University of Oxford, OX1 3QU Oxford, United Kingdom; [c]Department of Molecular Genetics and [d]Department of Biomolecular Sciences, Weizmann Institute of Science, 76100 Rehovot, Israel

ABSTRACT **Hereditary sensory and autonomic neuropathy (HSAN) types IA and IC (IA/C) are caused by elevated levels of an atypical class of lipid named 1-deoxysphingolipid (DoxSL). How elevated levels of DoxSL perturb the physiology of the cell and how the perturbations lead to HSAN IA/C are largely unknown. In this study, we show that C_{26}-1-deoxydihydroceramide (C_{26}-DoxDHCer) is highly toxic to the cell, while C_{16}- and C_{18}-DoxDHCer are less toxic. Genome-wide genetic screens and lipidomics revealed the dynamics of DoxSL accumulation and DoxSL species responsible for the toxicity over the course of DoxSL accumulation. Moreover, we show that disruption of F-actin organization, alteration of mitochondrial shape, and accumulation of hydrophobic bodies by DoxSL are not sufficient to cause complete cellular failure. We found that cell death coincides with collapsed ER membrane, although we cannot rule out other possible causes of cell death. Thus, we have unraveled key principles of DoxSL cytotoxicity that may help to explain the clinical features of HSAN IA/C.**

Monitoring Editor
Robert G. Parton
University of Queensland

Received: Jul 8, 2019
Revised: Aug 29, 2019
Accepted: Sep 4, 2019

INTRODUCTION

Hereditary sensory and autonomic neuropathy (HSAN) types IA and IC (A/C) are inherited diseases that mainly affect the sensory and autonomic functions of the peripheral nervous system. The clinical hallmark of the diseases is loss of pain and temperature sensations in the distal extremities. In some cases, it is accompanied by hypohidrosis (diminished sweating) (Auer-Grumbach, 2008). In general, the diseases have a late onset varying between the second and the fifth decade of life (Auer-Grumbach, 2008), although cases with a congenital or childhood onset have been reported (Houlden *et al.*, 2006; Suh *et al.*, 2014). The progression of the diseases is usually slow. As the diseases progress, the affected individuals often develop complications, such as ulcerative mutilations; muscle wasting and weakness; reduced motor functions; and spontaneous shooting, burning, and lancinating pains (Houlden *et al.*, 2006; Auer-Grumbach, 2008; Rotthier *et al.*, 2010), leading to severe physical disabilities.

HSAN IA/C are caused by autosomal dominant missense mutations in two essential genes, *SPTLC1* and *SPTLC2* (Rotthier *et al.*, 2012), respectively. The genes encode the two main subunits of serine palmitoyltransferase (SPT), which is the first enzyme regulating the flux of lipids in the sphingolipid (SL) biosynthesis pathway. SPT condenses palmitoyl-CoA with L-serine to produce a sphingoid base, 3-ketosphinganine, which is rapidly reduced to sphinganine (Sa). Sa can be acylated by ceramide (Cer) synthase to produce a Cer, dihydroceramide (DHCer), which can be modified further to generate more complex SLs. Alternatively, Sa can be phosphorylated and

This article was published online ahead of print in MBoC in Press (http://www.molbiolcell.org/cgi/doi/10.1091/mbc.E19-07-0364) on September 11, 2019.

Author contributions: A.G.H., J.T.H., and H.R. conceived the study; A.G.H. performed most of the experiments and the analyses; J.T.H. assisted A.G.H. in lipidomics; A.G.H. and M.M. performed the genetic screen of knockout and hypomorphic (DAmP) mutants under the supervision of M.S.; A.G.H., A.H.M., and B.K. performed the genetic screen of transposon-insertion mutants (SATAY); A.G.H. and H.R. wrote the manuscript; All authors read the manuscript and commented on it.

*Address correspondence to: Howard Riezman (howard.riezman@unige.ch).

Abbreviations used: Cer, ceramide; DHCer, dihydroceramide; DoxCer, 1-deoxyceramide; DoxDHCer, 1-deoxydihydroceramide; DoxmetDHCer, 1-deoxymethyldihydroceramide; DoxmetSa, 1-deoxymethylsphinganine; DoxSa, 1-deoxysphinganine; DoxSB, 1-deoxysphingoid base; DoxSL, 1-deoxysphingolipid; HSAN, hereditary sensory and autonomic neuropathy; MoA, mechanism of action; Sa, sphinganine; SATAY, saturated transposon analysis in yeast; SL, sphingolipid; SPT, serine palmitoyltransferase.

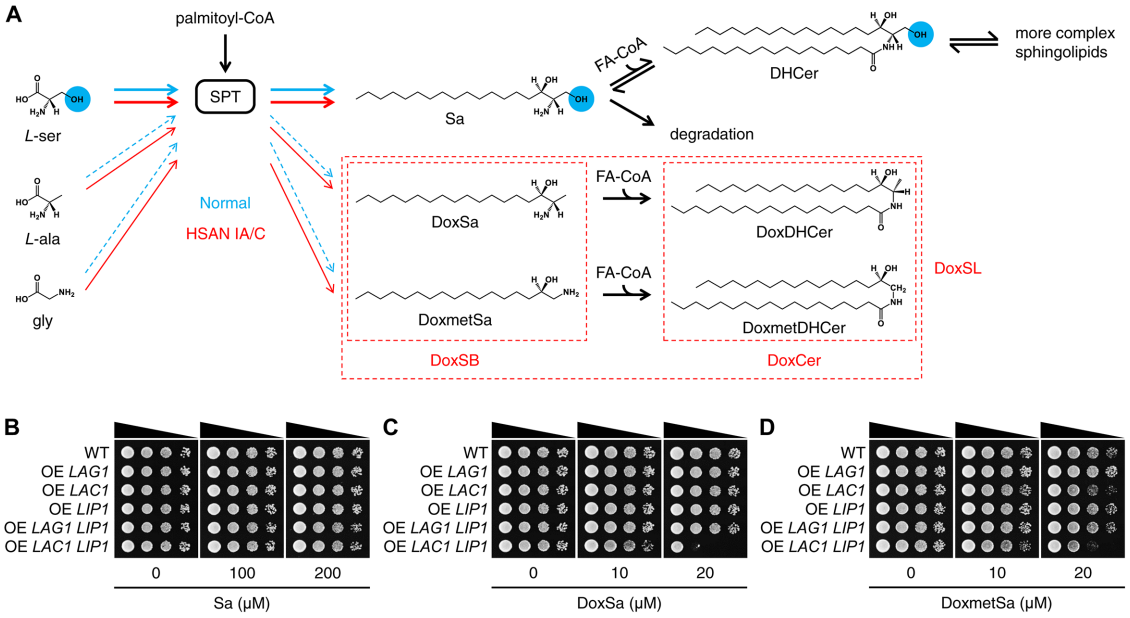

FIGURE 1: Elevated levels of DoxSL are toxic to yeast. (A) Schematic effect of HSAN IA/C mutations on the substrate promiscuity of SPT. The blue circles highlight the hydroxyl group that is missing in DoxSL. (B–D) Effect of sphingoid bases on the growth of the indicated strains evaluated by a spot assay. Sa, sphinganine; DoxSa, 1-deoxysphinganine; DoxmetSa, 1-deoxymethylsphinganine; DoxSB, 1-deoxysphingoid base; FA-CoA, fatty acyl-CoA; DHCer, dihydroceramide; DoxDHCer, 1-deoxydihydroceramide; DoxmetDHCer, 1-deoxymethyldihydroceramide; DoxCer, 1-deoxyceramide.

then degraded. The latter route constitutes the SL degradation pathway (Merrill, 2011; Megyeri *et al.*, 2016) (Figure 1A).

SPT can also use L-alanine or glycine as a substrate, albeit at much lower efficiency, to produce atypical sphingoid bases, 1-deoxysphinganine (DoxSa) or 1-deoxymethylsphinganine (DoxmetSa), respectively. Similar to Sa, DoxSa, and DoxmetSa can also be acylated by Cer synthase to form atypical Cers, 1-deoxydihydroceramide (DoxDHCer) and 1-deoxymethyldihydroceramide (DoxmetDHCer), respectively. In contrast to the typical SL, 1-deoxysphingolipid (DoxSL) lacks a hydroxyl group at the first carbon. Since the hydroxyl group is required for the synthesis of complex SLs and the degradation of SLs, DoxSL cannot progress in the pathway and tends to accumulate in the cell (Merrill, 2011). The mutations found in individuals with HSAN IA/C enhance the substrate promiscuity of SPT toward L-alanine and glycine (Gable *et al.*, 2010; Penno *et al.*, 2010), leading to increased synthesis and therefore accumulation of DoxSL, leading to HSAN IA/C (Figure 1A). How elevated levels of DoxSL perturb the physiology of the cell and how the perturbations lead to disease progression are largely unknown.

Studies in various mammalian cells showed that elevated levels of DoxSL perturb multiple components of the cell, including actin stress fibers (Cuadros *et al.*, 2000), mitochondria (Alecu *et al.*, 2017; Wilson *et al.*, 2018), and lipid droplets (Marshall *et al.*, 2014; Esaki *et al.*, 2015). However, to which extent the perturbations affect cell viability is unknown. An inhibitor of Cer synthase, Fumonisin B1 alleviates the toxic effects of DoxSL (Sanchez *et al.*, 2008; Zuellig *et al.*, 2014; Guntert *et al.*, 2016). In addition, the levels of $C_{22–24}$-1-deoxyceramide (DoxCer) in blood plasma associate with the incidence and severity of neuropathy caused by paclitaxel in cancer chemotherapy (Kramer *et al.*, 2015). These findings suggest that different species of DoxCer have different degrees of toxicity. Various pathways of DoxSL-induced cell death have been proposed, including ER stress-induced cell death (Gable *et al.*, 2010; Alecu *et al.*, 2017), aberrant Ca^{2+} homeostasis-induced apoptosis (Wilson *et al.*, 2018), noncanonical apoptosis (Salcedo *et al.*, 2007), and necrosis (Zuellig *et al.*, 2014).

In this study, we sought a comprehensive understanding of the cytotoxicity of DoxSL by genome-wide genetic screens and lipidomics. Given that elevated levels of DoxSL are toxic to various mammalian cells, worms (Hannich *et al.*, 2017), fruit flies (Oswald *et al.*, 2015), mice (Eichler *et al.*, 2009), and humans, we hypothesized that elevated levels of DoxSL are toxic to all eukaryotic cells in a conserved manner. Therefore, we used the budding yeast, *Saccharomyces cerevisiae* (hereafter termed yeast), as a simple eukaryotic model system to reveal the principles of DoxSL toxicity and the key DoxSL-induced perturbations that lead to cell death. By making use of the fatty acyl-CoA specificity of mammalian Cer synthase, we showed that C_{26}-DoxDHCer is more toxic than C_{16}- or C_{18}-DoxDHCer. Genome-wide genetic screens and lipidomics revealed the dynamics of DoxSL accumulation and DoxSL species responsible for the toxicity over the course of DoxSL accumulation. Furthermore, we showed that DoxSa accumulation leads to depletion of major membrane lipids. By standardizing the conditions of DoxSa treatment, we showed that disruption of F-actin organization, alteration of mitochondrial shape, and accumulation of hydrophobic bodies by DoxSL are not lethal under our conditions. We found that cell death coincides with a collapsed ER membrane, although we cannot rule out other possible causes of cell death. Thus, we have unraveled key principles of DoxSL cytotoxicity that can provide insights into the clinical features of HSAN IA/C.

RESULTS

Elevated levels of DoxSL are toxic to yeast

To test whether elevated levels of DoxSL are toxic to yeast, we compared the effect of the typical sphingoid base, Sa, with that of 1-deoxysphingoid base (DoxSB) on cell growth by a spot assay. To ensure that the formation of DoxCer from supplemented DoxSB is not limited by the endogenous Cer synthase, we overexpressed the

enzyme by integrating an additional copy of its gene with the constitutively active strong promoter of glyceraldehyde-3-phosphate dehydrogenase isozyme 3 (*TDH3*) into the yeast genome. Yeast Cer synthase may be composed of a Lag1p or Lac1p homodimer or a Lag1p-Lac1p heterodimer. Each of these dimers contains at least two copies of Lip1p, which is an essential protein required for the activity of yeast Cer synthase (Vallee and Riezman, 2005). Therefore, we also overexpressed *LIP1* in the same way.

The assay showed that Sa did not inhibit cell growth regardless of Cer synthase overexpression up to 200 μM (Figure 1B). In contrast to Sa, DoxSa was sufficient to strongly inhibit the growth of the strain overexpressing *LAC1 LIP1* (Figure 1C) at 20 μM. Similarly, DoxmetSa was also sufficient to inhibit the growth of the same strain at the same concentration, albeit to a lesser degree (Figure 1D). This result demonstrates that DoxSB is much more toxic than the typical sphingoid base and suggests that elevated levels of DoxCer are also toxic to yeast.

At the same concentration, however, DoxSa or DoxmetSa did not inhibit the growth of the strain overexpressing *LAG1 LIP1*. It is possible that Lag1p is less abundant than Lac1p because the expression level of *LAC1* is normally higher than that of *LAG1* (Kolaczkowski *et al.*, 2004) or that Lag1p is less efficient than Lac1p in converting DoxSB to DoxCer. The latter explanation is consistent with the recent finding that Lag1p prefers phytosphingosine to Sa as a substrate (Megyeri *et al.*, 2019) and therefore is expected to have reduced activity toward DoxSa or DoxmetSa.

C_{26}-DoxDHCer is more toxic than C_{16}- or C_{18}-DoxDHCer

To evaluate the toxicity of DoxCer species differing in the length of their acyl chain, we made use of the fatty acyl-CoA specificity of mammalian Cer synthase. There are six Cer synthases (CerS1–6) in mammals. Each enzyme uses specific fatty acyl-CoA species to produce corresponding Cer species (Levy and Futerman, 2010) (Figure 2A). We expressed individual mammalian Cer synthases in yeast to confer on yeast an ability to convert supplemented DoxSB to different DoxCer species. The enzymes were expressed by integrating their genes with the *TDH3* promoter into the yeast genome. Each of the expressed enzymes was able to support growth when the genes of yeast Cer synthase were deleted (Δ*lag1* Δ*lac1*), demonstrating that they all are functional in yeast (Supplemental Figure S1A). We then subjected the strains expressing mammalian Cer synthases in addition to the endogenous ones to a spot assay.

The assay showed that Sa at 200 μM did not inhibit the growth of WT and the strains expressing CerS1, 2, 3, or 4 and mildly inhibited the growth of the strains expressing CerS5 or 6 (Figure 2B). In contrast to Sa, DoxSa at 5 μM was sufficient to strongly inhibit the growth of the strain expressing CerS3. At 10 μM, DoxSa strongly inhibited the growth of the strains expressing CerS3, 5, or 6, but did not inhibit the growth of WT nor the strains expressing CerS1, 2, or 4 (Figure 2C). This result suggests that the toxicity of DoxDHCer depends on the length of its acyl chain. In contrast to DoxSa, DoxmetSa at 40 μM strongly inhibited the growth of WT and all strains to the same degree (Figure 2D). This result suggests either that mammalian Cer synthase expressed in yeast cannot convert DoxmetSa to DoxmetDHCer or that DoxmetSa is toxic on its own. Therefore, we cannot evaluate the toxicity of different DoxmetDHCer species.

To determine the species and the levels of accumulated DoxDHCer in cells for a given concentration of DoxSa, we treated the strains with DoxSa in a liquid medium at a nontoxic condition (low DoxSa concentration, high cell density, one yeast generation time) and then measured the levels of SL in the cells by mass spectrometry (MS). A nontoxic condition was chosen to ensure that the cells were not saturated with DoxDHCer, therefore allowing comparison between the levels of accumulated DoxDHCer in different strains. The MS analysis showed that DoxSa had a minor effect on the levels of typical SL (Supplemental Figure S1, B–H), demonstrating that the treatment condition is not toxic to the cells. The analysis also showed that following the DoxSa treatment, the strain expressing CerS3 mainly accumulated C_{26}-DoxDHCer. Interestingly, the level of C_{26}-DoxDHCer in the strain was much higher than that in WT, indicating that the mammalian CerS3, which makes the same DHCer species as the yeast Cer synthase, is more efficient in producing C_{26}-DoxDHCer than the yeast enzyme. Moreover, the level of C_{26}-DoxDHCer

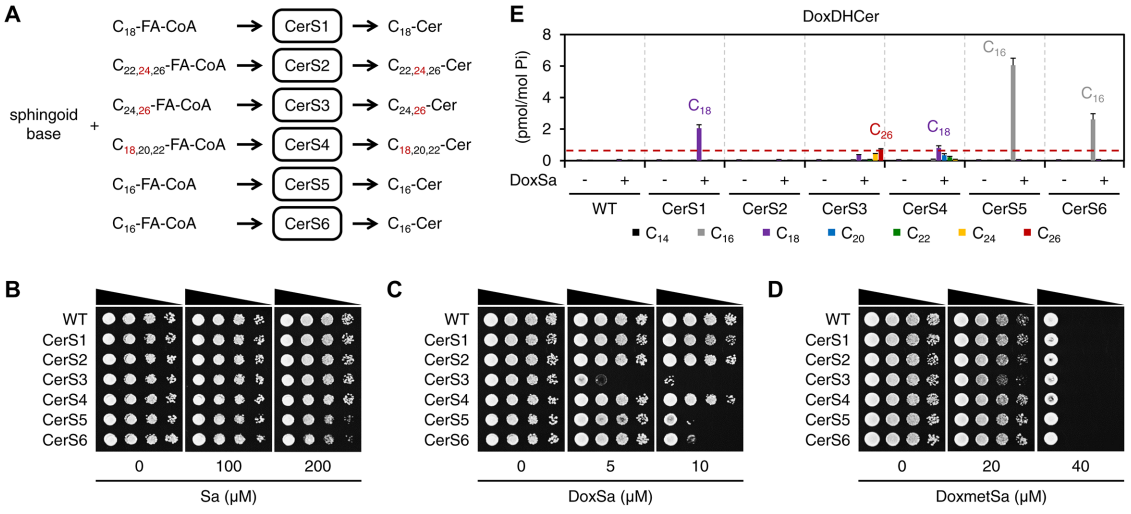

FIGURE 2: C_{26}-DoxDHCer is more toxic than C_{16}- or C_{18}-DoxDHCer. (A) Schematic representation of the fatty acyl-CoA specificity of mammalian Cer synthase. The red numbers indicate the major species of fatty acyl-CoA and Cer. (B–D) Effect of sphingoid bases on the growth of the indicated strains evaluated by a spot assay. (E) Levels of DoxDHCer species in the indicated strains without or with a nontoxic DoxSa treatment (2 μM of DoxSa, 20 million cells/ml, 1.5 h) determined by MS. The red dashed line indicates the level of C_{26}-DoxDHCer in the CerS3 strain following the treatment; $n = 3$.

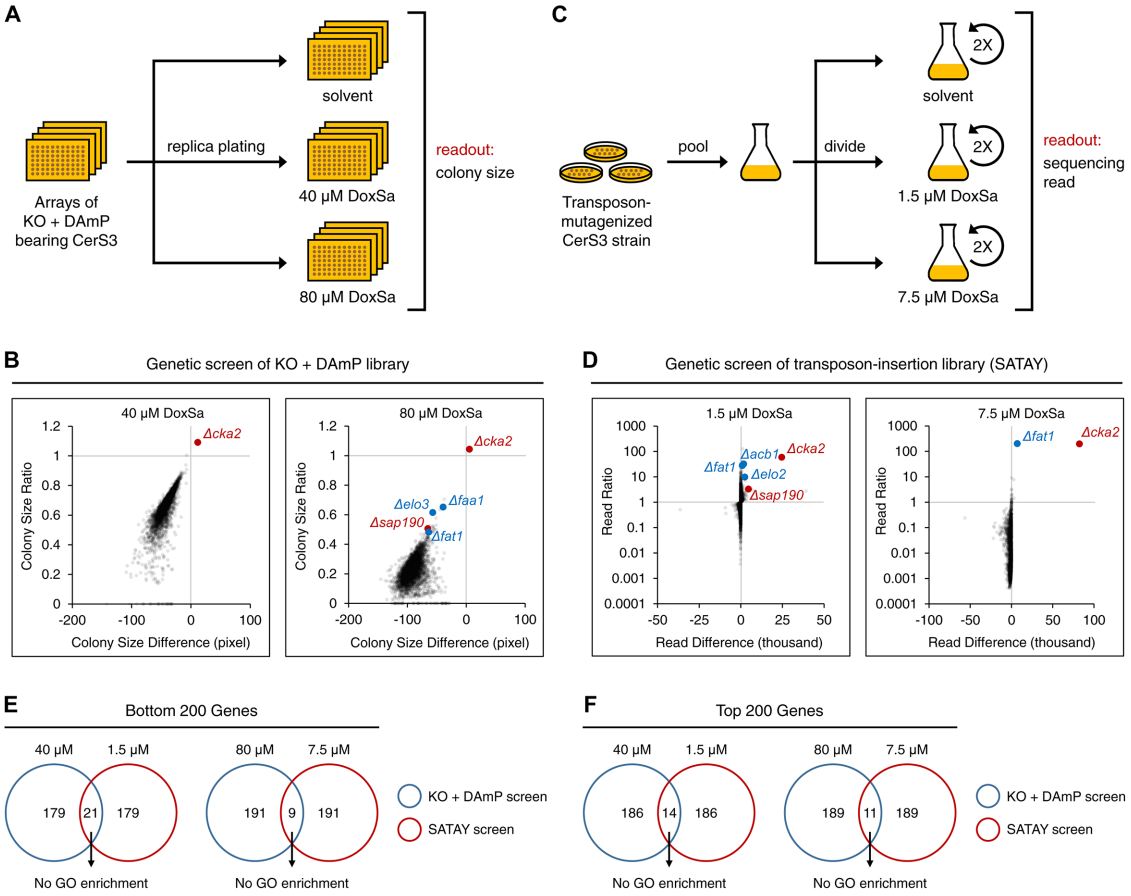

FIGURE 3: Genome-wide genetic screens to reveal the MoA of DoxSL. (A) Schematic workflow of genome-wide genetic screen of knockout and DAmP mutants. (B) Changes in colony size of the mutants following a DoxSa treatment at the indicated concentrations; $n = 2$. (C) Schematic workflow of genome-wide genetic screen of transposon-insertion mutants (SATAY). (D) Changes in sequencing read of the mutants following a DoxSa treatment at the indicated concentrations; $n = 2$. (E, F) Proportions of genes that were in the bottom (E) or top (F) 200 of the fitness ranks and that were revealed by the two genetic screens. There is no GO enrichment in each set of genes.

in the strain was lower than those of C_{16}-DoxDHCer in the strains expressing CerS5 or 6 and those of C_{18}-DoxDHCer in the strains expressing CerS1 or 4 (Figure 2E). Nevertheless, the strain expressing CerS3 was the strain most sensitive to DoxSa (Figure 2C). These results strongly indicate that C_{26}-DoxDHCer is more toxic than C_{16}- or C_{18}-DoxDHCer.

Genome-wide genetic screen of knockout and hypomorphic (DAmP) mutants

To gain insights into the mechanism of action (MoA) of DoxSL, we performed a genome-wide genetic screen for gene products whose absence or deficiency renders the cell hypersensitive or resistant to DoxSL. We decided to focus on DoxSa and DoxDHCer for two reasons. First, we have more information about the effect of acyl chain length on the toxicity of DoxDHCer than that of DoxmetDHCer. Second, we could minimize the amount of DoxSa consumed for the screen by using the strain expressing CerS3, which is the strain most sensitive to DoxSa, as a background strain. The screen was performed by first introducing CerS3 into every single yeast strain in the knockout or DAmP allele library using automated approaches (Tong and Boone, 2006; Cohen and Schuldiner, 2011). Then, the resulting library, in which each strain expressed CerS3 and had one mutant allele, was replica plated onto an agar medium supplemented with different concentrations of DoxSa. Two concentrations were chosen, such that hypersensitive or resistant mutants were revealed prominently at the lower or the higher concentration, respectively. Colony size was scored as a measure of fitness of the mutants (Figure 3A).

The library covered 79.5% of nonessential genes and 68.8% of essential genes (Supplemental Figure S2A). Quality control assessments revealed that the extents of biases and technical variabilities in the screen were below our tolerance limits (Supplemental Figure S2, B–F). The screen revealed that deletion of genes that are required for efficient import of sphingoid base (Δ*faa1*) or synthesis of very long-chain fatty acyl-CoA (Δ*elo3*, Δ*fat1*) rendered the cell resistant to DoxSa (Figure 3B). Since efficient synthesis of C_{26}-DoxDHCer from DoxSa requires the two processes, this finding validates that changes in fitness of the mutants in the screen were mainly due to the high toxicity of C_{26}-DoxDHCer.

Gene ontology (GO) enrichment analysis of resistant genes (defined as genes whose Z-score of colony size ratio > 3, Z-score of solvent-treated colony size > –3.5, CV of colony size ratio < the 50% percentile) using the GOrilla tool (Eden *et al.*, 2007, 2009) showed that there is no enrichment of particular molecular functions, cellular components, or biological processes. Moreover, physical and genetic-interaction density analysis (Dittmar *et al.*, 2013) was unable to reveal groups of functionally related hypersensitive or resistant genes. In addition, examination of individual hypersensitive or resistant genes failed to reveal a clear hypothesis of the MoA of DoxSL.

During the examination of individual genes, we found that the identities of about 10% of the mutants in the library could not be confirmed by colony PCR. Furthermore, several freshly generated mutants failed to show the same responses to DoxSa as those indicated by the result of the screen. These findings raised a concern that the mutants in the library had accumulated too many suppressors, thus preventing us from obtaining insights into the MoA of DoxSL.

Genome-wide genetic screen of transposon-insertion mutants (SATAY)

To ensure that we did not miss key gene products involved in the MoA of DoxSL, we decided to perform another genome-wide genetic screen with an independent method in which the library is freshly-generated. The method is termed SAturated Transposon Analysis in Yeast (SATAY) (Michel *et al.*, 2017). The screen was performed by first inducing random insertion of a transposon from a plasmid into the genome of the CerS3 strain. The mutagenesis was performed in a large number of cells to generate a saturated transposon-insertion library. Then, the library was divided and subjected to a two-round treatment with DoxSa at different concentrations. Two concentrations were chosen for the same purpose as that in the screen of knockout and DAmP mutants. The number of deep sequencing reads was used as a measure of fitness of the mutants (Figure 3C).

The transposon insertion mutated 91.5% of nonessential genes and 52.5% of essential genes (Supplemental Figure S3A). The number of transposon insertion sites of most genes remained unchanged following DoxSa treatment at the lower concentration (Supplemental Figure S3B), suggesting that the complexity of the library was maintained during the screening procedure and that technical variabilities had little impact on the result of the screen. The screen revealed that disruption of genes that are required for synthesis of very long-chain fatty acyl-CoA and its presentation to the Cer synthase (Δ*fat1*, Δ*acb1*, Δ*elo2*) rendered the cell resistant to DoxSa (Figure 3D). This finding validates that changes in fitness of the mutants in the screen were mainly due to the high toxicity of C_{26}-DoxDHCer.

We performed various data analyses ranging from enrichment analyses to examination of individual transposon insertion sites. Furthermore, we scrutinized genes that were in the bottom or top 200 of the fitness ranks and that were revealed by the two genetic screens (Figure 3, E and F). However, once again, we were unable to formulate a clear hypothesis of the MoA of DoxSL. To allow independent analyses of the data sets by others, all primary data are published here (Supplemental Tables S1 and S2). It is possible that the MoA cannot be revealed by genetic screens in which gene products are deleted, disrupted, or reduced. Therefore, we performed a multicopy suppressor screen for gene products whose overproduction alleviates the toxicity of DoxSL. In this screen, the CerS3 strain was transformed with a pool of plasmids, each of which carried four to five genes and the 2-micron sequence that maintains a high copy number of the plasmid in the cell. Then, the transformed cells were subjected to a three-round treatment with DoxSa at different concentrations. We found that cultures treated with high concentrations of DoxSa did not gain noticeable density after the second and the third round of treatment (unpublished data). Considering that the plasmid library covers 97.2% of the yeast genome with 5.4-fold depth of coverage (Jones *et al.*, 2008) and that the transformed cells covered the plasmid library with 15.9-fold depth of coverage, this finding suggests that there is no single gene whose overexpression is capable of alleviating the toxicity of DoxSL.

Given the results of the three genetic screens, we hypothesized two possibilities of the MoA of DoxSL. 1) DoxSL inhibits an essential multisubunit protein complex and the inhibition cannot be suppressed by deletion or overproduction of another protein. 2) DoxSL inhibits multiple proteins and pathways, such that perturbing any single one does not reveal the full MoA. This inhibition could be achieved directly or indirectly, such as by affecting the physical properties of cellular membranes.

The dynamics of DoxSL species responsible for the toxicity over the course of DoxSL accumulation

To gain more insights into the toxicity of DoxSL, we subjected the deletion mutants of the resistant genes required for efficient import of sphingoid base or synthesis of very long-chain fatty acyl-CoA, along with those of two resistant genes, *CKA2* (encoding alpha catalytic subunit of casein kinase 2) and *SAP190* (encoding a component of type 2A-related serine-threonine phosphatase SIT4) to a spot assay and to MS analysis following the nontoxic DoxSa treatment.

The assay showed that all mutants were more resistant, to different degrees, to DoxSa at 5 μM than the parent strain (the CerS3 strain) (Figure 4A). The MS analysis showed that all mutants accumulated less C_{26}-DoxDHCer than the CerS3 strain following the DoxSa treatment (Figure 4B). It also showed that C_{26}-DoxDHCer was the only DoxDHCer species whose accumulation levels in all mutants were lower than that in the CerS3 strain (Supplemental Figure S4, A–F). Therefore, the degrees of resistance of the mutants could be

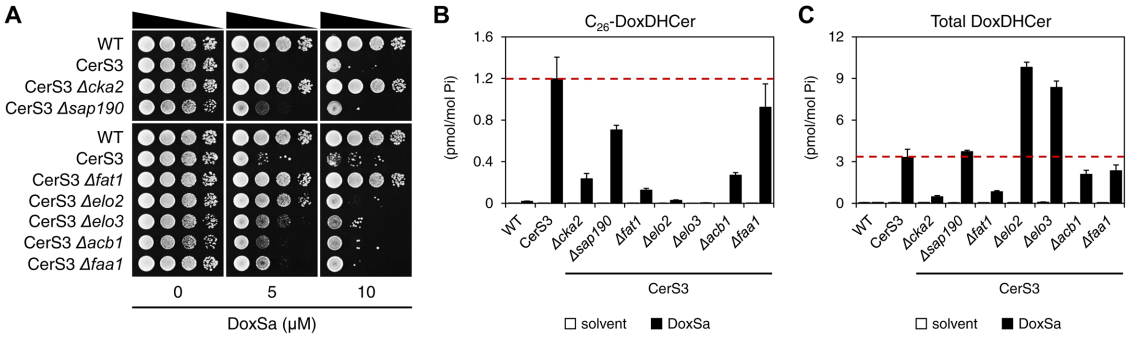

FIGURE 4: The dynamics of DoxSL species responsible for the toxicity over the course of DoxSL accumulation. (A) Effect of DoxSa on the growth of the indicated strains evaluated by a spot assay. (B, C) Levels of C_{26}-DoxDHCer (B) and total DoxDHCer (C) in the indicated strains without or with a nontoxic DoxSa treatment (2 μM of DoxSa, 20 million cells/ml, 1.5 h) determined by MS. The red dashed lines indicate the levels of C_{26}-DoxDHCer and total DoxDHCer in the CerS3 strain following the treatment; $n = 3$.

attributed to their ability to suppress the accumulation of C_{26}-DoxDHCer. However, the degree of resistance and the ability to suppress the accumulation of C_{26}-DoxDHCer of the mutants did not correlate perfectly, suggesting that C_{26}-DoxDHCer was not the only toxic DoxSL species. This became more apparent at a higher concentration of DoxSa. The degrees of resistance of the mutants at 10 μM of DoxSa (Figure 4A) could not be explained by their ability to suppress the accumulation of C_{26}-DoxDHCer (Figure 4B). Instead, they could be better explained by their ability to suppress the accumulation of all DoxDHCer species, albeit imperfectly (Figure 4C).

The results indicate that the toxicity of DoxSL is the summed toxicity of DoxSa and individual DoxDHCer species. The results also show that the DoxSL species responsible for the toxicity varies depending on the amount of DoxSL that accumulates. When DoxSL is present at low levels, its toxic effects are mainly caused by the most toxic DoxDHCer species (C26-DoxDHCer). When DoxSL is present at high levels, its toxic effects cannot be attributed to one main species as the toxic effects of DoxSa and the other DoxDHCer species become more evident.

Standardizing conditions of DoxSa treatment for phenotypic characterization

To gain more insights into the toxicity of DoxSL, we characterized the phenotypes of DoxSL toxicity. To this end, we first standardized conditions of DoxSa treatment by testing the effect of various concentrations of DoxSa, durations of DoxSa treatment, and cell densities on cell viability. We aimed to obtain a range of DoxSa concentrations that gives a wide range of cell viabilities after one yeast generation time (1.5 h). One generation time was chosen to maximize the effects of DoxSL while minimizing the compounding effects of intergeneration events and the depletion of DoxSa from the medium. We treated cells at low cell densities to maximize their sensitivity to DoxSL. Following a treatment, cells were washed and spotted on an agar medium to assay their ability to recover. We found that treating WT and the CerS3 strain with DoxSa at concentrations of 0, 2, 4, and 6 μM for 1.5 h, at a cell density of 1 million cells/ml gave a wide range of cell viabilities (Figure 5A). Therefore, we used these conditions of DoxSa treatment for the phenotypic characterization.

Disruption of F-actin organization is not sufficient to cause cell death

DoxSa treatment was shown to reduce the presence of actin stress fibers in a mammalian cell line (Cuadros *et al.*, 2000). To test whether DoxSa treatment also disrupts F-actin organization in yeast, we performed confocal microscopy using phalloidin-Atto488 as a stain for F-actin. The microscopy showed that 4 μM of DoxSa for 1.5 h was sufficient to depolarize actin patches and markedly reduce the presence of actin cables and actin patches in WT. Moreover, it induced the formation of multiple micron-sized round bodies that could be stained with phalloidin-Atto488. The microscopy also showed that a lower concentration (2 μM of DoxSa) for 1.5 h gave the same phenotype in the CerS3 strain, albeit to a lesser degree (Figure 5, B and F). This result shows that DoxSa treatment disrupts F-actin organization in yeast. However, 4 μM of DoxSa for 1.5 h was not sufficient to block the recovery of WT cells (Figure 5A), demonstrating that the phenotype is not sufficient to cause cell death.

Alteration of mitochondrial shape is not sufficient to cause cell death

DoxSa treatment was shown to induce mitochondrial fragmentation, induce the loss of mitochondrial cristae, reduce respiration, and reduce ATP production in a mammalian cell line (Alecu *et al.*, 2017). To test whether DoxSa treatment also perturbs mitochondria in yeast, we performed confocal microscopy of strains expressing mCherry tagged-mitochondrial malate dehydrogenase (*MDH1-mCherry*). The microscopy showed that 4 μM of DoxSa for 1.5 h was sufficient to fragment mitochondria and alter the shape of mitochondria from tubular to spherical without affecting their inheritance from the mother cell to the bud in WT. The microscopy also showed that 2 μM of DoxSa for 1.5 h gave the same phenotype in the CerS3 strain, albeit to a lesser degree (Figure 5, C and G). This result shows that DoxSa treatment perturbs mitochondria in yeast. However, 4 μM of DoxSa for 1.5 h was not sufficient to prevent the recovery of WT cells (Figure 5A), demonstrating that the phenotype is not sufficient to cause cell death. Although the mitochondrial phenotype was dramatic, depletion of oxygen, nonfermentable carbon sources, or deletion of mitochondrial DNA did not modulate the sensitivity of WT and the CerS3 strain to DoxSa (Supplemental Figure S5, A–F). These results suggest that the phenotype is independent of mitochondrial respiration.

Accumulation of hydrophobic bodies is not sufficient to cause cell death

Mammalian cells lacking de novo biosynthesis of L-serine and HSAN IA patient-derived lymphoblasts were shown to have more lipid droplets than normal cells (Marshall *et al.*, 2014; Esaki *et al.*, 2015). To test whether DoxSa treatment also enhances the formation of lipid droplets in yeast, we performed confocal microscopy using a hydrophobic dye, Nile Red. The microscopy showed that 4 μM of DoxSa for 1.5 h was sufficient to markedly induce the formation of Nile Red-stained structures whose sizes, shapes, subcellular locations, and sharpness of the boundaries are distinct from those of lipid droplets (Figure 5D). The structures could also be observed in a quadruple mutant lacking the abilities to synthesize triglycerides and sterol esters (Δ*are1* Δ*are2* Δ*dga1* Δ*lro1*) following DoxSa treatment (Supplemental Figure S6, A and B), demonstrating that the formation of the structures is independent of neutral lipids and that they are not the canonical lipid droplets. Therefore, we call the structures "hydrophobic bodies." The microscopy also showed that 2 μM of DoxSa for 1.5 h gave the same phenotype in the CerS3 strain, albeit to a lesser degree (Figure 5, D and H). These results show that DoxSa treatment induces the formation of hydrophobic bodies in yeast. However, 4 μM of DoxSa for 1.5 h was not sufficient to prevent recovery of WT cells (Figure 5A), demonstrating that the phenotype is not sufficient to cause cell death.

Collapsed ER membrane coincides with cell death

Since the conversion of DoxSa to DoxDHCer presumably occurs at the ER membrane, where Cer synthase resides (Barz and Walter, 1999; Vallee and Riezman, 2005), we tested the effect of DoxSa treatment on the ER membrane by confocal microscopy of strains expressing GFP tagged-translocon (*SEC61-GFP*). The microscopy showed that 6 μM of DoxSa for 1.5 h was required to markedly collapse the cortical ER in WT. The microscopy also showed that 4 μM of DoxSa for 1.5 h was sufficient to induce more severe collapsed cortical ER in the CerS3 strain (Figure 5, E and I). This result shows that DoxSa treatment causes the ER membrane to collapse in yeast. In contrast to the other phenotypes, marked collapse of the cortical ER correlated with a marked reduction of cell viability (Figure 5, A and E), demonstrating that collapsed ER membrane coincides with cell death.

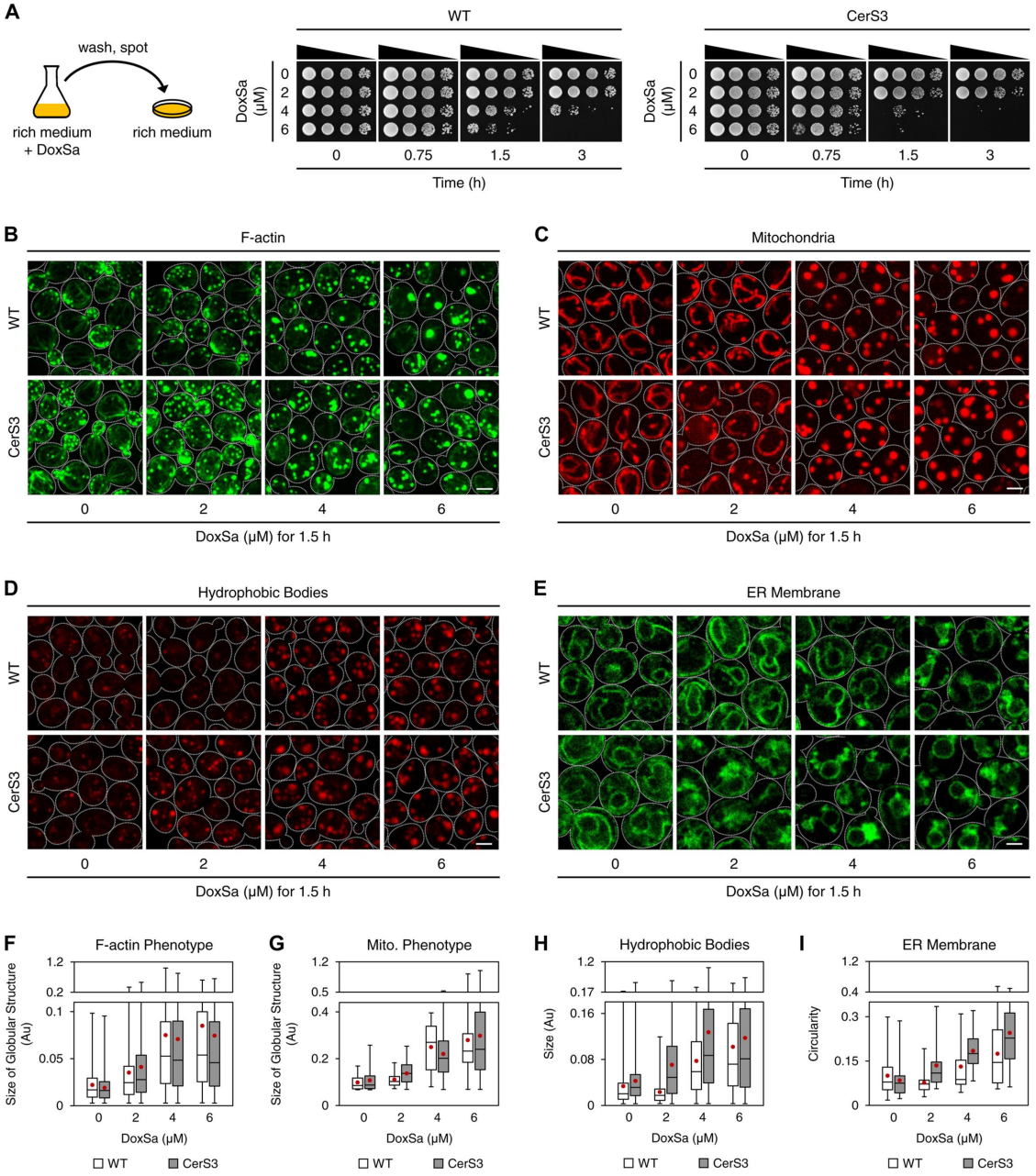

FIGURE 5: Cellular phenotypes of DoxSL toxicity. (A) Ability of WT and the CerS3 strain to recover from the indicated DoxSa treatments. (B–E) Cellular phenotypes of DoxSL toxicity. Organization of F-actin (B), shape of mitochondria (C), hydrophobic bodies (D), and the ER membrane (E) in WT and the CerS3 strain following standardized DoxSa treatments (indicated concentrations of DoxSa, 1 million cells/ml, 1.5 h). F-actin was stained with phalloidin-Atto488. Mitochondria were visualized with Mdh1p-mCherry. Hydrophobic bodies were stained with Nile Red. The ER membrane was visualized with Sec61p-GFP. Each image is a maximum intensity projection of a 2-μm slice. The scale bars are 2 μm. (F–I) Size of globular structures stained with phalloidin-Atto488 (F), size of globular structures highlighted by Mdh1p-mCherry (G), size of hydrophobic bodies (H), or circularity (a value of 1.0 indicates a perfect circle) of the ER membrane (I) in WT and the CerS3 strain following the standardized DoxSa treatments. Black bars indicate medians, boxes indicate quartiles, whiskers indicate extreme values, and red dots indicate means. Numbers of images used for the quantification: two to six.

We also tested the effects of DoxSa treatment on the nuclear envelope, the vacuolar membrane, the peroxisomal membrane, and the plasma membrane by confocal microscopy. However, we could not observe apparent morphological changes of the membranes (unpublished data), indicating that different cellular membranes are affected by elevated levels of DoxSL to different degrees.

DoxSa accumulation leads to depletion of major membrane lipids

To gain more insights into the toxicity of DoxSL, we performed lipidomics of WT and the CerS3 strain following the same DoxSa treatments as those for the phenotypic characterization by MS. The lipidomics showed that increased concentrations of DoxSa were accompanied by decreased levels of major membrane lipids in both

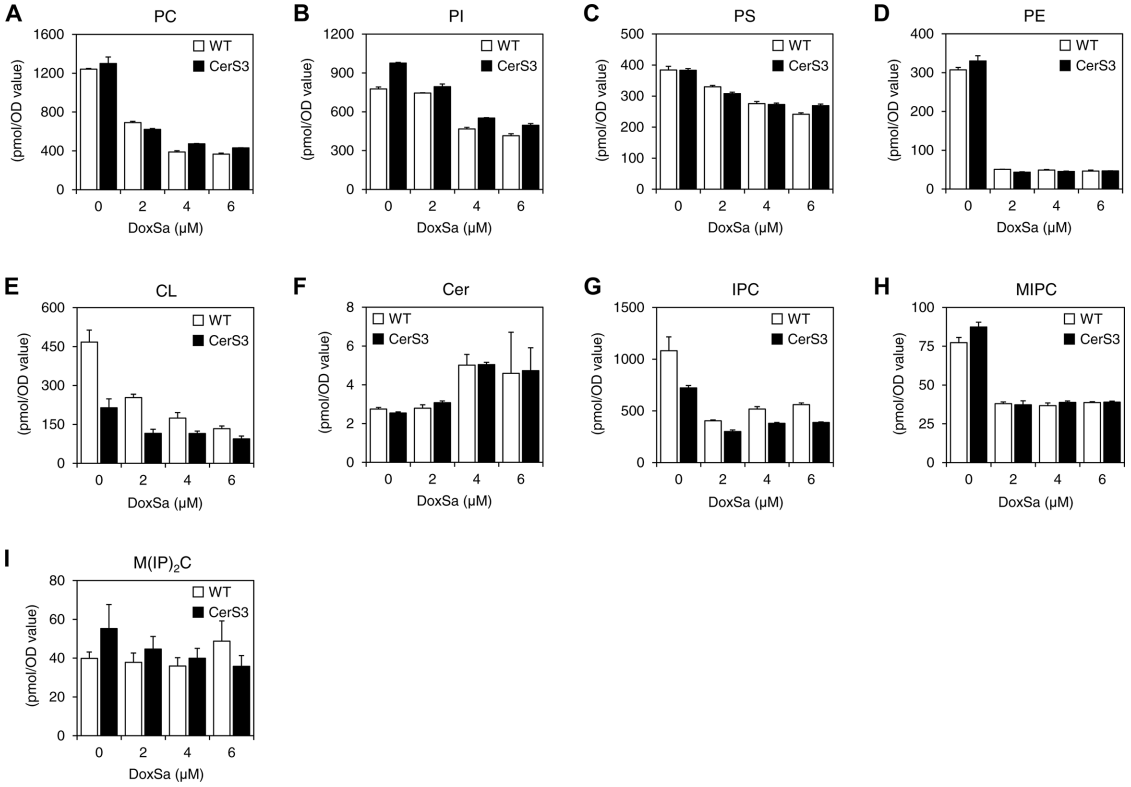

FIGURE 6: DoxSa accumulation leads to depletion of major membrane lipids. Levels of different categories of phospholipid (A–E) and SL (F–I) in WT and the CerS3 strain following the standardized DoxSa treatments (indicated concentrations of DoxSa, 1 million cells/ml, 1.5 h) determined by MS. PC, phosphatidylcholine; PI, phosphatidylinositol; PS, phosphatidylserine; PE, phosphatidylethanolamine; CL, cardiolipin; Cer, ceramide; IPC, inositol-phosphoceramide; MIPC, mannose-inositol-phosphoceramide; $M(IP)_2C$, mannose-(inositol-P)$_2$-ceramide; $n = 3$.

WT and the CerS3 strain. The lipids were five classes of glycerophospholipid (PC, PI, PS, PE, and CL) (Figure 6, A–E) and two classes of complex SLs (IPC and MIPC) (Figure 6, G and H). In contrast, increased concentrations of DoxSa were accompanied by increased levels of a SL intermediate, Cer (Figure 6F). Compared to those of other lipid classes, the levels of a class of complex SL, $M(IP)_2C$ were the least affected by increased concentrations of DoxSa (Figure 6I). Given that the degrees of depletion of the major membrane lipids in WT were comparable to those in the CerS3 strain, this result suggests that DoxSa, not DoxDHCer, accumulation leads to depletion of major membrane lipids.

The dynamics of DoxSL accumulation: the rate of DoxSa accumulation determines the level of DoxDHCer accumulation

The lipidomics also showed that increased concentrations of DoxSa were accompanied by increased levels of C_{26}-DoxDHCer and total DoxDHCer in the CerS3 strain and, to lesser degrees, in WT. In the CerS3 strain, we uncovered an unexpected phenomenon in which 2 μM of DoxSa resulted in higher levels of C_{26}-DoxDHCer and total DoxDHCer than 4 or 6 μM of DoxSa (Figure 7, A and B). A time-course lipid analysis by MS following a DoxSa treatment at 6 μM for up to 3 h showed that the longer the DoxSa treatment, the higher the levels of C_{26}-DoxDHCer and total DoxDHCer (Figure 7, C and D), demonstrating that the phenomenon is not due to postcell death events. In addition, deletion of ceramidase (Δ*ypc1* Δ*ydc1*) did not modulate the sensitivity of the CerS3 strain to DoxSa (Figure 7E), demonstrating that the phenomenon is ceramidase-independent. The phenomenon suggests the dynamics of DoxSL accumulation—that is to say, the rate of DoxSa accumulation determines the level of DoxDHCer accumulation. When the rates of DoxSa accumulation are high, the toxic effects of DoxSa rapidly manifest, thereby hindering further synthesis and accumulation of DoxDHCer. When the rates of DoxSa accumulation are low, the toxic effects of DoxSa never or slowly manifest, thereby allowing continuous or prolonged synthesis and accumulation of DoxDHCer. Since CerS3 allows efficient conversion of DoxSa to DoxDHCer, the phenomenon is more apparent in the CerS3 strain.

Model of the cytotoxicity of DoxSL

Since the phenotypes in the CerS3 strain were more severe than those in WT following a given DoxSa treatment (Figure 5, B–I), the phenotypes could not be fully attributed to elevated levels of DoxSa and depletion of major membrane lipids (Figure 6, A–I). Also, since the levels of accumulated DoxDHCer did not fully correlate with the severity of the phenotypes (Figures 5, B–I, and 7, A and B), the phenotypes could not be fully attributed to elevated levels of DoxDHCer either. Therefore, the phenotypes must be caused by elevated levels of both DoxSa and DoxDHCer. Furthermore, deletion of the ER-to-plasma membrane tethers was shown to cause a similarly collapsed ER membrane phenotype without causing cell death in yeast (Manford *et al.*, 2012). Therefore, it is likely that in this case as well, the collapsed ER membrane is not sufficient to cause cell death, although it coincides with cell death.

Collectively, our findings suggest the following model of the cytotoxicity of DoxSL. Elevated levels of both DoxSa and DoxDHCer disrupt the organization of F-actin, alter the shape of mitochondria, induce the formation of hydrophobic bodies, and cause the ER

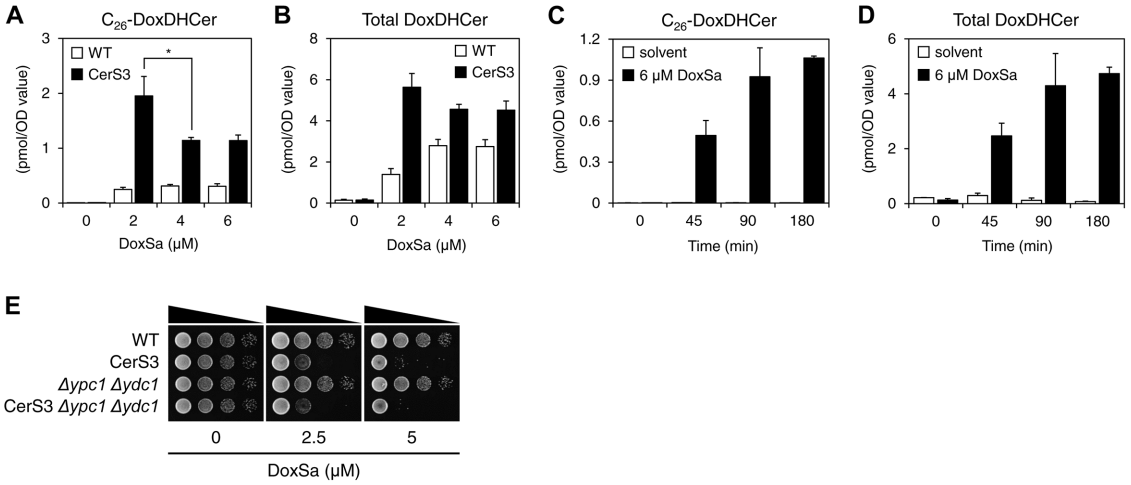

FIGURE 7: The rate of DoxSa accumulation determines the level of DoxDHCer accumulation. Levels of C_{26}-DoxDHCer (A) and total DoxDHCer (B) in WT and the CerS3 strain following the standardized DoxSa treatments (indicated concentrations of DoxSa, 1 million cells/ml, 1.5 h) determined by MS; $n = 3$. (C, D) Levels of C_{26}-DoxDHCer (C) and total DoxDHCer (D) in the CerS3 strain monitored by a time-course lipid analysis by MS following a DoxSa treatment at 6 μM for up to 3 h; $n = 2$. (E) Effect of DoxSa on the growth of the indicated strains evaluated by a spot assay. Deletion of ceramidase (Δ*ypc1* Δ*ydc1*) did not modulate the sensitivity of the CerS3 strain to DoxSa, indicating that the accumulation of DoxDHCer is independent of ceramidase.

membrane to collapse. The first three perturbations precede cell death, indicating that they are not sufficient to cause complete cellular failure. The last perturbation coincides with cell death, which might suggest that it is one of the final perturbations in DoxSL-induced cell death. Nevertheless, we cannot rule out other possible causes of cell death (Figure 8). Considering that 1) DoxSa and individual DoxDHCer species might have different mechanisms of action and that 2) the perturbations are expected to negatively affect multiple proteins and pathways, this model is more consistent with our second hypothesis formulated from the results of the three genetic screens.

DISCUSSION

In this study, we took comprehensive approaches to the cytotoxicity of DoxSL. Gradual accumulation of DoxSL underlies late-onset slowly progressing neurological diseases HSAN IA/C. In addition, elevated levels of DoxSL have been implicated in other diseases, such as type 2 diabetes, diabetic sensory neuropathy, von Gierke disease, and nonalcoholic hepatosteatosis (Lone *et al.*, 2019). Therefore, unraveling the cytotoxicity of DoxSL is key to understanding the pathogenesis of HSAN IA/C and the roles of DoxSL in the other diseases.

We found that C_{26}-DoxDHCer is more toxic to the cell than C_{16}- or C_{18}-DoxDHCer. It is possible that C_{26}-DoxDHCer is the most toxic DoxSL species. In humans, very long-chain ($C_{22–26}$) Cers are synthesized by CerS3, which is highly expressed in skin cells (Levy and Futerman, 2010). Therefore, we hypothesize that 1) skin cells should be directly affected by elevated levels of DoxSL and that 2) unhealthy skin cells are contributors to the origin of this clinical hallmark and other clinical features of HSAN IA/C.

Our findings might provide explanations to key questions regarding the clinical hallmark of HSAN IA/C. 1) What causes loss of pain and temperature sensation? A study in zebrafish showed that epithelial damage precedes degeneration of sensory axons (Lisse *et al.*, 2016). This finding suggests that unhealthy skin cells might lead to degeneration of sensory neurons innervating the skin. 2) Why are sensory functions more affected than motor functions? Skeletal muscles mainly express CerS1 and 5, which produce C18- and C16-DoxDHCer, respectively (Levy and Futerman, 2010). Therefore, skeletal muscles and neuromuscular junctions would be less affected than skin cells and nociceptors in the skin. Affected individuals might also suffer from hypohidrosis (diminished sweating) (Auer-Grumbach, 2008) and recurrent chronic skin ulcers that heal very slowly (up to a year). Such ulcers might develop from minor wounds that heal very slowly (Auer-Grumbach, 2008) or without an apparent cause (Denny-Brown, 1951). These clinical features led us to hypothesize that unhealthy skin cells might perturb adjacent sweat glands and contribute to the ulcers.

Eight missense mutations in *SPTLC1* and six missense mutations in *SPTLC2* have been conclusively linked to HSAN IA/C,

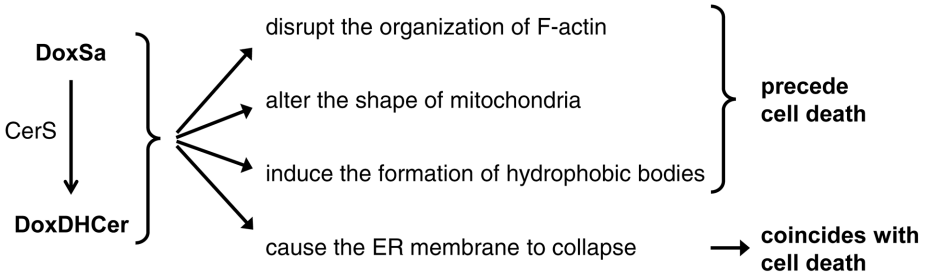

FIGURE 8: Model of the cytotoxicity of DoxSL. Elevated levels of both DoxSa and DoxDHCer disrupt the organization of F-actin, alter the shape of mitochondria, induce the formation of hydrophobic bodies, and cause the ER membrane to collapse. The first three perturbations are not sufficient to cause complete cellular failure. The last perturbation coincides with cell death. This model is consistent with the hypothesis that DoxSL inhibits a multisubunit essential protein affecting multiple pathways. Alternatively, DoxSL could inhibit multiple pathways, directly or indirectly, such as by affecting the physical properties of cellular membranes.

respectively (Bode *et al.*, 2016; Suriyanarayanan *et al.*, 2016, 2019). Different mutations increase the substrate promiscuity of SPT toward L-alanine and glycine to different degrees, leading to different accumulation rates of DoxSB (Bode *et al.*, 2016). We found that low accumulation rates of DoxSa allow slow accumulation of DoxDHCer for long periods of time until DoxDHCer reaches its toxic level, whereas high accumulation rates of DoxSa lead to brief periods of DoxDHCer production as DoxSa rapidly reaches its toxic level. We also found that the DoxDHCer species responsible for the toxicity of DoxDHCer change over the course of its accumulation. The most toxic species (C_{26}-DoxDHCer) is mainly responsible for the toxicity when the levels of DoxDHCer are low, whereas all species are responsible for the toxicity when the levels of DoxDHCer are high. Since individual DoxSB and DoxCer species might have different mechanisms of action, our findings suggest that 1) the mechanism of cytotoxicity might vary in affected individuals with different causing mutations and that 2) it might evolve over the course of the development of the disease.

Finally, this study highlights the importance of acyl chain length in the toxicity of DoxDHCer. Since individual DoxSB and DoxCer species might have different mechanisms of action, further studies should be focused on dissecting the toxicity of individual DoxSB and DoxCer species.

MATERIALS AND METHODS

Yeast strains

The yeast strains used in this study are listed in Table 1.

Lipids

The lipids used were Sa (Avanti 860498), DoxSa (Avanti 860493), and DoxmetSa (Avanti 860473). The lipids were dissolved in ethanol and sonicated for 5 min using an ultrasonic bath to make stock solutions. The solutions were stored at –20°C. Before use, the solutions were brought to room temperature and sonicated for 5 min.

Spot assay

YPD agar supplemented with 10 mM of MES, 0.05% (vol/vol) of Tergitol NP-40, and a lipid was prepared 2 d in advance. On the spotting day, cells were suspended at a 10-fold serial dilution with OD_{600} of 1.5 at the highest in 200 µl of YPD liquid in a U-bottom 96-well plate. The cells were spotted on the agar medium using a 48-pin tool. The culture was incubated at 30°C for 2 d.

Lipidomics analysis

DoxSa treatment. Exponentially growing cells (OD_{600} of 1 or 20 million cells/ml for nontoxic DoxSa treatment, or OD_{600} of 0.05 or 1 million cells/ml for the standardized DoxSa treatment) in YPD liquid were treated with DoxSa at 30°C for the indicated durations. Then, the metabolism of the cells was immediately quenched with 5% of ice-cold trichloroacetic acid.

Lipid extraction. Lipid extraction was performed as described before (da Silveira Dos Santos *et al.*, 2014) with minor modifications. Briefly, a mixture of lipid standards (7.5 nmol of 17:0/14:1 PC, 7.5 nmol of 17:0/14:1 PE, 6 nmol of 17:0/14:1 PI, 4 nmol of 17:0/14:1 PS, 1.2 nmol of C_{17}- Cer, 1.2 nmol of C_{12}- DoxDHCer, and 2 nmol of C_8-glucosylceramide) was added to 25 OD_{600} values of cells. Then, the cells were subjected to two rounds of lipid extraction with 1.5 ml of extraction solvent (ethanol, water, diethyl ether, pyridine, 4.2 N of ammonium hydroxide 15:15:5:1:0.018) and 250 µl of glass beads by vigorous vortexing for 5 min followed by incubation at 60°C for 20 min. Cell debris was pelleted at 800 × *g* for 5 min, and the supernatant was collected. The combined supernatant was divided into two equal aliquots for glycerolipid and SL analyses. Both aliquots were dried with a stream of nitrogen. The SL aliquot was then treated with 0.5 ml of monomethylamine reagent (methanol, water, *n*-butanol, methylamine 4:3:1:5) at 53°C for 1 h and dried again. Next, both dried aliquots were subjected to three rounds of desalting by resuspending them in 300 µl of water-saturated *n*-butanol and 150 µl of water followed by centrifugation at 3200 × *g* for 10 min to induce phase separation. The upper phases were collected. To start another round of desalting, the lower phase was mixed again with 300 µl of water-saturated *n*-butanol. The combined upper phases were dried and stored at –80°C.

MS. The dried lipid extracts were dissolved in 500 µl of chloroform:methanol (1:1). Each extract was diluted with chloroform:methanol:water (2:7:1) or chloroform:methanol (1:2) containing 5 mM of ammonium acetate for positive- or negative-mode MS, respectively. Then, the samples were infused into a TSQ Vantage mass spectrometer (ThermoFisher) using a Nanomate (Advion) with a gas pressure of 30 psi and a spray voltage of 1.2 kV for multiple reaction monitoring analyses. The mass spectrometer was operated with a spray voltage of 3.5 kV in positive mode and 3 kV in negative mode. The capillary temperature was set to 190°C. Lipid amounts were normalized by the amounts of inorganic phosphate or OD_{600} values of cells.

Genome-wide genetic screen of knockout and DAmP mutants

Synthetic genetic array (SGA). The CerS3 strain (in yMS721 background) was used as a donor strain to introduce the gene into every strain in the knockout or DAmP allele library (Giaever *et al.*, 2002; Breslow *et al.*, 2008) by the SGA method (Tong and Boone, 2006; Cohen and Schuldiner, 2011). Briefly, the CerS3 strain was pinned onto 1536-format arrays of mutant colonies on YPD agar using a pinning robot (Singer Instruments) and incubated at room temperature for 1 d to induce mating. Then, the cells were pinned onto SD MSG agar–Ura + 200 mg/ml of G418 and incubated at 30°C for 1 d to select for diploid cells. The selection was repeated once. Next, the cells were pinned onto SPO agar and incubated at room temperature for 5 d to induce sporulation. The plates were wrapped with a moist towel to prevent desiccation. Then, the cells were pinned onto SD MSG agar–His/Lys/Arg/Ura + 50 mg/l of canavanine + 50 mg/l of thialysine and incubated at 30°C for 2 d to select for cells with the same mating type as that of the mutants. Next, the cells were pinned onto SD MSG agar–His/Lys/Arg/Ura + 50 mg/l of canavanine + 50 mg/l of thialysine + 200 mg/ml of G418 and incubated at 30°C for 1 d to select for the mutants bearing CerS3. The selection was repeated once. The library was maintained on the same medium without G418.

DoxSa treatment and colony size measurement. The cells in the library were pinned onto SD MSG agar–His/Lys/Arg/Ura + 50 mg/l of canavanine + 50 mg/l of thialysine + 0.05% (vol/vol) of Tergitol NP-40 supplemented with DoxSa and incubated at 30°C for 1 d. Then, the plates were scanned with a paper scanner (Hewlett Packard). The size of colonies was determined with the "Balony" software (Young and Loewen, 2013) by including the row-column correction.

Genome-wide genetic screen of transposon-insertion mutants (SATAY)

Library generation. SATAY was performed as described before (Michel *et al.*, 2017) with minor modifications. Briefly, the SATAY

No.	Name	Genotype	Source
1	WT (yMS721)	MATα*his3Δ1 leu2Δ0 lys2+/lys+ met15Δ0 ura3Δ0 can1Δ::STE2pr-sp HIS5 lyp1Δ::STE3pr-LEU2*	Maya Schuldiner
2	OE *LAG1*	yMS721 *TDH3pr-LAG1-CYC1term URA3*	This study (RH8147)
3	OE *LAC1*	yMS721 *TDH3pr-LAC1-CYC1term URA3*	This study (RH8148)
4	OE *LIP1*	yMS721 *TDH3pr-LIP1-CYC1term URA3*	This study (RH8149)
5	OE *LAG1 LIP1*	yMS721 *TDH3pr-LAG1-CYC1termTDH3pr-LIP1-CYC1term* (tandem) *URA3*	This study (RH8150)
6	OE *LAC1 LIP1*	yMS721 *TDH3pr-LAC1-CYC1termTDH3pr-LIP1-CYC1term* (tandem) *URA3*	This study (RH8151)
7	CerS1	yMS721 *TDH3pr-CERS1-CYC1term URA3*	This study (RH8152)
8	CerS2	yMS721 *TDH3pr-CERS2-CYC1term URA3*	This study (RH8153)
9	CerS3	yMS721 *TDH3pr-CERS3-CYC1term URA3*	This study (RH8154)
10	CerS4	yMS721 *TDH3pr-CERS4-CYC1term URA3*	This study (RH8155)
11	CerS5	yMS721 *TDH3pr-CERS5-CYC1term URA3*	This study (RH8156)
12	CerS6	yMS721 *TDH3pr-CERS6-CYC1term URA3*	This study (RH8157)
13	WT (BY4741)	MATa *his3Δ1 leu2Δ0 met15Δ0 ura3Δ0*	Howard Riezman (RH8039)
14	KO and DAmP library	BY4741 *KanMX4*	Maya Schuldiner
15	SATAY CerS3	BY4741 *TDH3pr-CERS3-CYC1term KanMX6 ade2Δ::HIS3*	This study (RH8158)
16	CerS3	BY4741 *TDH3pr-CERS3-CYC1term URA3*	This study (RH8159)
17	CerS3 Δ*cka2*	BY4741 CerS3 *cka2Δ::LEU2*	This study (RH8160)
18	CerS3 Δ*sap190*	BY4741 CerS3 *sap190Δ::LEU2*	This study (RH8161)
19	CerS3 Δ*fat1*	BY4741 CerS3 *fat1Δ::LEU2*	This study (RH8162)
20	CerS3 Δ*elo2*	BY4741 CerS3 *elo2Δ::LEU2*	This study (RH8163)
21	CerS3 Δ*elo3*	BY4741 CerS3 *elo3Δ::LEU2*	This study (RH8164)
22	CerS3 Δ*acb1*	BY4741 CerS3 *acb1Δ::LEU2*	This study (RH8165)
23	CerS3 Δ*faa1*	BY4741 CerS3 *faa1Δ::LEU2*	This study (RH8166)
24	WT Mdh1p-mCherry	BY4741 *MDH1-mCherry KanMX4*	This study (RH8167)
25	CerS3 Mdh1p-mCherry	BY4741 CerS3 *MDH1-mCherry KanMX4*	This study (RH8168)
26	WT Sec61p-GFP	BY4741 *SEC61-GFP HIS3*	This study (RH8169)
27	CerS3 Sec61p-GFP	BY4741 CerS3 *SEC61-GFP HIS3*	This study (RH8170)
28	WT (HR2885)	MATα*Δhis3 Δleu2 Δura3 Δlys2 Δade2 Δtrp1 Δbar1*	Howard Riezman (RH2885)
29	Δ*lag1* Δ*lac1*	HR2885 *lag1Δ::HIS3 lac1Δ::ADE2*	Howard Riezman (RH7165)
30	Δ*lag1* Δ*lac1* CerS1	Δ*lag1* Δ*lac1 TDH3pr-CERS1-CYC1term TRP1*	Howard Riezman (RH7911)
31	Δ*lag1* Δ*lac1* CerS2	Δ*lag1* Δ*lac1 TDH3pr-CERS2-CYC1term TRP1*	Howard Riezman (RH7912)
32	Δ*lag1* Δ*lac1* CerS3	Δ*lag1* Δ*lac1 TDH3pr-CERS3-CYC1term TRP1*	Howard Riezman (RH7913)
33	Δ*lag1* Δ*lac1* CerS4	Δ*lag1* Δ*lac1 TDH3pr-CERS4-CYC1term TRP1*	Howard Riezman (RH7914)
34	Δ*lag1* Δ*lac1* CerS5	Δ*lag1* Δ*lac1 TDH3pr-CERS5-CYC1term TRP1*	Howard Riezman (RH7915)
35	Δ*lag1* Δ*lac1* CerS6	Δ*lag1* Δ*lac1 TDH3pr-CERS6-CYC1term TRP1*	Howard Riezman (RH7916)
36	WT rho^0 (ρ^0)	BY4741 rho^0 (ρ^0)	This study (RH8171)
37	CerS3 rho0 (ρ0)	BY4741 CerS3 rho^0 (ρ^0)	This study (RH8172)
38	Quadruple mutant	Δ*are1* Δ*are2* Δ*dga1* Δ*lro1*	Stephen Sturley (RH6106) Barnard College, Columbia University
39	Δ*ypc1* Δ*ydc1*	BY4741 *ypc1Δ::KanMX6 ydc1Δ::HphMX4 pep4Δ::LEU2*	This study (RH8173)
40	CerS3 Δ*ypc1* Δ*ydc1*	BY4741 CerS3 *ypc1Δ::KanMX6 ydc1Δ::HphMX4 pep4Δ::LEU2*	This study (RH8174)

TABLE 1: Yeast strains used in this study.

CerS3 strain was transformed with pBK257 plasmid containing the transposon. Freshly transformed cells were inoculated into 1 l of SC liquid + 0.2% of glucose + 2% of raffinose–Ura at OD_{600} of 0.15 and grown at 30°C until saturation (OD_{600} of 3–4). Then, the culture was concentrated 10 times by centrifugation at 600 × *g* for 5 min to obtain final OD_{600} of 37. To induce transposition, the cells were

plated using glass beads onto 433 8.5-cm Petri dishes of SC agar + 2% of galactos–Ade and incubated at 30°C for 3 wk. Contaminated plates were removed during the incubation time. Next, colonies were scraped using a glass rod with minimum amounts of SC liquid + 2% of glucose–Ade, pooled, inoculated into 1 l of SC liquid + 2% of glucose–Ade at OD_{600} of 0.125, and incubated at 30°C until OD_{600} of 0.5. The library was used immediately.

DoxSa treatment. The cells in the library were pelleted at 800 × *g* for 5 min, inoculated into prewarmed 500 ml of SC liquid + 2% of glucose–Ade supplemented with DoxSa at OD_{600} of 0.1, and incubated at 30°C until saturation. The treatment was repeated once. Next, the cells were harvested by centrifugation at 2500 × *g*, 4°C, for 5 min and stored at –80°C.

DNA preparation. Genomic DNA of about 500 mg of cells was extracted by the phenol/chloroform extraction method. Next, 2 µg of genomic DNA was digested with 50 U of *Dpn*II or *Nla*III at 37°C for 24 h. The enzymes were then heat inactivated at 65°C for 20 min. The DNA fragments were circularized with 25 Weiss U of T4 ligase at 22°C for 6 h. The circularized DNA molecules were precipitated with 0.3 M of sodium acetate, pH 5.2, 1 ml of ethanol, and 5 µg linear acrylamide (Ambion AM9520) at –20°C overnight. Then, DNA was pelleted at 16,100 × *g*, 4°C, for 20 min, washed with 1 ml of 70% ethanol, and dried at 37°C for 10 min. Next, transposon fragments were amplified with Taq polymerase (New England Biolabs). The PCR products were then purified with the PCR clean-up/gel extraction kit (Macherey-Nagel) according to the manufacturer's instruction, with the following modifications. DNA was bound to the column by centrifugation at 3000 × *g* for 30 s. Then, 30 µl of elution buffer (10 mM Tris-HCl, pH 8.5, 0.1% [vol/vol] Tween 20) was applied to the column, incubated for 3 min, and eluted by centrifugation at 11,000 × *g*, 20°C, for 1 min. The eluate was reapplied to the column and a second elution was performed under the same conditions.

Deep sequencing. Equal amounts of DNA from *Dpn*II- and *Nla*III-digested samples were pooled and sequenced using MiSeq v3 chemistry, according to the manufacturer's instruction.

Fluorescence microscopy

F-actin. Exponentially growing cells (OD_{600} of 0.05 or 1 million cells/ml) in YPD liquid were treated with DoxSa and incubated at 30°C for 1.5 h. Next, the cells were fixed by directly adding paraformaldehyde to the culture at a final concentration of 4%. Then, 1 OD_{600} value of cells were washed with 3 ml of washing buffer (0.1 M of potassium phosphate, pH 7.5, 1.2 M of sorbitol), stained with 50 µl of 1 µM of phalloidin-Atto488 (Sigma-Aldrich) at 4°C for 1 h in the dark, and observed by confocal microscopy. The severity of the F-actin phenotype was measured as the area of globular structures stained with phalloidin-Atto488.

Mitochondria. Exponentially growing cells expressing Mdh1p-mCherry in YPD liquid were treated with DoxSa and incubated at 30°C for 1.5 h. Next, the cells were observed by confocal microscopy immediately without fixation. The severity of the mitochondria phenotype was measured as the area of globular structures highlighted by Mdh1p-mCherry.

Hydrophobic bodies. Exponentially growing cells in YPD liquid were treated with DoxSa and incubated at 30°C for 1.5 h. Next, the cells were fixed by directly adding paraformaldehyde to the culture at a final concentration of 4%. Then, 1 OD_{600} value of cells were washed with 3 ml of the washing buffer, stained with 1 µl of 1 mg/ml Nile Red at 4°C for 15 min in the dark, and observed by confocal microscopy. The size of a hydrophobic body was measured as the area of the structure stained with Nile Red.

The ER membrane. Exponentially growing cells expressing Sec61p-GFP in YPD liquid were treated with DoxSa and incubated at 30°C for 1.5 h. Next, the cells were observed by confocal microscopy immediately without fixation. The severity of the ER membrane phenotype was measured as the circularity of the ER membrane. The circularity of the ER membrane was calculated as 4π*area/perimeter^2. A value of 1.0 indicates a perfect circle. As the value approaches 0.0, it indicates an increasingly elongated shape.

Anaerobic culture

Cells were spotted onto an anaerobic (supplemented with 10 mg/l of ergosterol and 420 mg/l of Tween 80) YPD, YPEG, or YPL agar medium. The Petri dish was placed inside an airtight chamber (ThermoFisher) equipped with a pack of oxygen-consuming reagent (ThermoFisher) and oxygen color indicators (ThermoFisher). The chamber was closed immediately and incubated at 30°C for 3 d.

Generating rho^0 (ρ^0) cells

Exponentially growing cells in SD liquid were treated with 25 µg/ml of ethidium bromide from OD_{600} of 0.1 until saturation (24 h). The step was repeated twice.

Growth curve assay

Cells were suspended at OD_{600} of 0.1 in 200 µl of YPD liquid in a flat-bottom 96-well plate. The cover of the plate was replaced with a gas permeable seal (4titude 4ti-0516-96). The culture was incubated at 30°C with agitation for 24 h in a plate reader (Biotek Synergy H1) while OD_{600} of the culture was recorded every 10 min.

ACKNOWLEDGMENTS

A.G.H., M.M., M.S., and H.R. were supported by the EU ITN "Sphingonet." A.G.H. was supported by the Institute of Genetics and Genomics of Geneva (iGE3). A.H.G., J.T.H., and H.R. were supported by NCCR Chemical Biology and the Swiss National Science Foundation. M.S. is an incumbent of the Dr. Gilbert Omenn and Martha Darling Professorial Chair in Molecular Genetics. M.S. is also supported by a VW foundation LIFE grant. A.H.M. and B.K. were supported by the European Research Council (Starting Grant 337906-OrgaNet).

REFERENCES

Alecu I, Tedeschi A, Behler N, Wunderling K, Lamberz C, Lauterbach MA, Gaebler A, Ernst D, Van Veldhoven PP, Al-Amoudi A, *et al.* (2017). Localization of 1-deoxysphingolipids to mitochondria induces mitochondrial dysfunction. J Lipid Res 58, 42–59.

Auer-Grumbach M (2008). Hereditary sensory neuropathy type I. Orphanet J Rare Dis 3, 7.

Barz WP, Walter P (1999). Two endoplasmic reticulum (ER) membrane proteins that facilitate ER-to-Golgi transport of glycosylphosphatidylinositol-anchored proteins. Mol Biol Cell 10, 1043–1059.

Bode H, Bourquin F, Suriyanarayanan S, Wei Y, Alecu I, Othman A, Von Eckardstein A, Hornemann T (2016). HSAN1 mutations in serine palmitoyltransferase reveal a close structure-function-phenotype relationship. Hum Mol Genet 25, 853–865.

Breslow DK, Cameron DM, Collins SR, Schuldiner M, Stewart-Ornstein J, Newman HW, Braun S, Madhani HD, Krogan NJ, Weissman JS (2008). A comprehensive strategy enabling high-resolution functional analysis of the yeast genome. Nat Methods 5, 711–718.

Cohen Y, Schuldiner M (2011). Advanced methods for high-throughput microscopy screening of genetically modified yeast libraries. Methods Mol Biol 781, 127–159.

Cuadros R, Montejo de Garcini E, Wandosell F, Faircloth G, Fernandez-Sousa JM, Avila J (2000). The marine compound spisulosine, an inhibitor of cell proliferation, promotes the disassembly of actin stress fibers. Cancer Lett 152, 23–29.

da Silveira Dos Santos AX, Riezman I, Aguilera-Romero MA, David F, Piccolis M, Loewith R, Schaad O, Riezman H (2014). Systematic lipidomic analysis of yeast protein kinase and phosphatase mutants reveals novel insights into regulation of lipid homeostasis. Mol Biol Cell 25, 3234–3246.

Denny-Brown D (1951). Hereditary sensory radicular neuropathy. J Neurol Neurosurg Psychiatry 14, 237–252.

Dittmar JC, Pierce S, Rothstein R, Reid RJ (2013). Physical and genetic-interaction density reveals functional organization and informs significance cutoffs in genome-wide screens. Proc Natl Acad Sci USA 110, 7389–7394.

Eden E, Lipson D, Yogev S, Yakhini Z (2007). Discovering motifs in ranked lists of DNA sequences. PLoS Comput Biol 3, e39.

Eden E, Navon R, Steinfeld I, Lipson D, Yakhini Z (2009). GOrilla: a tool for discovery and visualization of enriched GO terms in ranked gene lists. BMC Bioinformatics 10, 48.

Eichler FS, Hornemann T, McCampbell A, Kuljis D, Penno A, Vardeh D, Tamrazian E, Garofalo K, Lee HJ, Kini L, *et al.* (2009). Overexpression of the wild-type SPT1 subunit lowers desoxysphingolipid levels and rescues the phenotype of HSAN1. J Neurosci 29, 14646–14651.

Esaki K, Sayano T, Sonoda C, Akagi T, Suzuki T, Ogawa T, Okamoto M, Yoshikawa T, Hirabayashi Y, Furuya S (2015). L-Serine deficiency elicits intracellular accumulation of cytotoxic deoxysphingolipids and lipid body formation. J Biol Chem 290, 14595–14609.

Gable K, Gupta SD, Han G, Niranjanakumari S, Harmon JM, Dunn TM (2010). A disease-causing mutation in the active site of serine palmitoyltransferase causes catalytic promiscuity. J Biol Chem 285, 22846–22852.

Giaever G, Chu AM, Ni L, Connelly C, Riles L, Veronneau S, Dow S, Lucau-Danila A, Anderson K, Andre B, *et al.* (2002). Functional profiling of the Saccharomyces cerevisiae genome. Nature 418, 387–391.

Guntert T, Hanggi P, Othman A, Suriyanarayanan S, Sonda S, Zuellig RA, Hornemann T, Ogunshola OO (2016). 1-Deoxysphingolipid-induced neurotoxicity involves N-methyl-d-aspartate receptor signaling. Neuropharmacology 110, 211–222.

Hannich JT, Mellal D, Feng S, Zumbuehl A, Riezman H (2017). Structure and conserved function of iso-branched sphingoid bases from the nematode Caenorhabditis elegans. Chem Sci 8, 3676–3686.

Houlden H, King R, Blake J, Groves M, Love S, Woodward C, Hammans S, Nicoll J, Lennox G, O'Donovan DG, *et al.* (2006). Clinical, pathological and genetic characterization of hereditary sensory and autonomic neuropathy type 1 (HSAN I). Brain 129, 411–425.

Jones GM, Stalker J, Humphray S, West A, Cox T, Rogers J, Dunham I, Prelich G (2008). A systematic library for comprehensive overexpression screens in Saccharomyces cerevisiae. Nat Methods 5, 239–241.

Kolaczkowski M, Kolaczkowska A, Gaigg B, Schneiter R, Moye-Rowley WS (2004). Differential regulation of ceramide synthase components LAC1 and LAG1 in Saccharomyces cerevisiae. Eukaryot Cell 3, 880–892.

Kramer R, Bielawski J, Kistner-Griffin E, Othman A, Alecu I, Ernst D, Kornhauser D, Hornemann T, Spassieva S (2015). Neurotoxic 1-deoxysphingolipids and paclitaxel-induced peripheral neuropathy. FASEB J 29, 4461–4472.

Levy M, Futerman AH (2010). Mammalian ceramide synthases. IUBMB Life 62, 347–356.

Lisse TS, Middleton LJ, Pellegrini AD, Martin PB, Spaulding EL, Lopes O, Brochu EA, Carter EV, Waldron A, Rieger S (2016). Paclitaxel-induced epithelial damage and ectopic MMP-13 expression promotes neurotoxicity in zebrafish. Proc Natl Acad Sci USA 113, E2189–E2198.

Lone MA, Santos T, Alecu I, Silva LC, Hornemann T (2019). 1-Deoxysphingolipids. Biochim Biophys Acta 1864, 512–521.

Manford AG, Stefan CJ, Yuan HL, Macgurn JA, Emr SD (2012). ER-to-plasma membrane tethering proteins regulate cell signaling and ER morphology. Dev Cell 23, 1129–1140.

Marshall LL, Stimpson SE, Hyland R, Coorssen JR, Myers SJ (2014). Increased lipid droplet accumulation associated with a peripheral sensory neuropathy. J Chem Biol 7, 67–76.

Megyeri M, Prasad R, Volpert G, Sliwa-Gonzalez A, Galih A, Aguilera-Romero A, Riezman H, Barral Y, Futerman AH, Schuldiner M (2019). Yeast ceramide synthases, Lag1 and Lac1, have distinct substrate specificity. J Cell Sci 132, jcs228411.

Megyeri M, Riezman H, Schuldiner M, Futerman AH (2016). Making sense of the yeast sphingolipid pathway. J Mol Biol 428, 4765–4775.

Merrill AH Jr. (2011). Sphingolipid and glycosphingolipid metabolic pathways in the era of sphingolipidomics. Chem Rev 111, 6387–6422.

Michel AH, Hatakeyama R, Kimmig P, Arter M, Peter M, Matos J, De Virgilio C, Kornmann B (2017). Functional mapping of yeast genomes by saturated transposition. Elife 6, e23570.

Oswald MC, West RJ, Lloyd-Evans E, Sweeney ST (2015). Identification of dietary alanine toxicity and trafficking dysfunction in a Drosophila model of hereditary sensory and autonomic neuropathy type 1. Hum Mol Genet 24, 6899–6909.

Penno A, Reilly MM, Houlden H, Laura M, Rentsch K, Niederkofler V, Stoeckli ET, Nicholson G, Eichler F, Brown RH Jr, *et al.* (2010). Hereditary sensory neuropathy type 1 is caused by the accumulation of two neurotoxic sphingolipids. J Biol Chem 285, 11178–11187.

Rotthier A, Auer-Grumbach M, Janssens K, Baets J, Penno A, Almeida-Souza L, Van Hoof K, Jacobs A, De Vriendt E, Schlotter-Weigel B, *et al.* (2010). Mutations in the SPTLC2 subunit of serine palmitoyltransferase cause hereditary sensory and autonomic neuropathy type I. Am J Hum Genet 87, 513–522.

Rotthier A, Baets J, Timmerman V, Janssens K (2012). Mechanisms of disease in hereditary sensory and autonomic neuropathies. Nat Rev Neurol 8, 73–85.

Salcedo M, Cuevas C, Alonso JL, Otero G, Faircloth G, Fernandez-Sousa JM, Avila J, Wandosell F (2007). The marine sphingolipid-derived compound ES 285 triggers an atypical cell death pathway. Apoptosis 12, 395–409.

Sanchez AM, Malagarie-Cazenave S, Olea N, Vara D, Cuevas C, Diaz-Laviada I (2008). Spisulosine (ES-285) induces prostate tumor PC-3 and LNCaP cell death by de novo synthesis of ceramide and PKCzeta activation. Eur J Pharmacol 584, 237–245.

Suh BC, Hong YB, Nakhro K, Nam SH, Chung KW, Choi BO (2014). Early-onset severe hereditary sensory and autonomic neuropathy type 1 with S331F SPTLC1 mutation. Mol Med Rep 9, 481–486.

Suriyanarayanan S, Auranen M, Toppila J, Paetau A, Shcherbii M, Palin E, Wei Y, Lohioja T, Schlotter-Weigel B, Schon U, *et al.* (2016). The variant p.(Arg183Trp) in SPTLC2 causes late-onset hereditary sensory neuropathy. Neuromolecular Med 18, 81–90.

Suriyanarayanan S, Othman A, Dräger B, Schirmacher A, Young P, Mulahasanovic L, Hörtnagel K, Biskup S, von Eckardstein A, Hornemann T, *et al.* (2019). A novel variant (Asn177Asp) in SPTLC2 causing hereditary sensory autonomic neuropathy type 1C. Neuromolecular Med 21, 182–191.

Tong AH, Boone C (2006). Synthetic genetic array analysis in Saccharomyces cerevisiae. Methods Mol Biol 313, 171–192.

Vallee B, Riezman H (2005). Lip1p: a novel subunit of acyl-CoA ceramide synthase. EMBO J 24, 730–741.

Wilson ER, Kugathasan U, Abramov AY, Clark AJ, Bennett DLH, Reilly MM, Greensmith L, Kalmar B (2018). Hereditary sensory neuropathy type 1-associated deoxysphingolipids cause neurotoxicity, acute calcium handling abnormalities and mitochondrial dysfunction in vitro. Neurobiol Dis 117, 1–14.

Young BP, Loewen CJ (2013). Balony: a software package for analysis of data generated by synthetic genetic array experiments. BMC Bioinformatics 14, 354.

Zuellig RA, Hornemann T, Othman A, Hehl AB, Bode H, Guntert T, Ogunshola OO, Saponara E, Grabliauskaite K, Jang JH, *et al.* (2014). Deoxysphingolipids, novel biomarkers for type 2 diabetes, are cytotoxic for insulin-producing cells. Diabetes 63, 1326–1339.